ARTICLE

All-Graphene Photodetectors

Freddie Withers, Thomas Hardisty Bointon, Monica Felicia Craciun, and Saverio Russo*

Centre for Graphene Science, College of Engineering, Mathematics, and Physical Sciences, University of Exeter, Exeter EX4 4QL, United Kingdom

ABSTRACT We investigate the optoelectronic properties of novel graphene/$FeCl_3$-intercalated few-layer graphene ($FeCl_3$—FLG, dubbed graphexeter) heterostructures using photovoltage spectroscopy. We observe a prominent photovoltage signal generated at the graphene/$FeCl_3$—FLG and graphene/Au interfaces, whereas the photovoltage at the $FeCl_3$—FLG/Au interface is negligible. The sign of the photovoltage changes upon sweeping the chemical potential of the pristine graphene through the charge neutrality point, and we show that this is due to the photothermoelectric effect. Our results are a first step toward all-graphene-based photodetectors and photovoltaics.

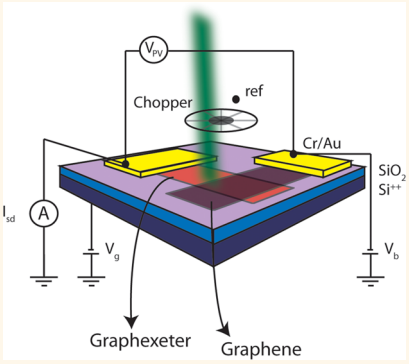

KEYWORDS: ferric chloride · intercalated · graphene · photovoltage · photodetector · optoelectronics

Harvesting energy from photons is of tremendous societal importance since it contributes to reduce the carbon footprint. In common photovoltaic devices, the conversion from photons into electrical voltage is accomplished exploiting the in-built electric field at the interface of a p- and n-doped semiconductor to separate the photogenerated electron—hole pairs and originate a forward photovoltage. However, the intrinsic band gap of standard semiconductors restricts the photoresponsivity of these devices to specific light bandwidths. To harvest electricity over a wide range of the sun light spectrum, the multijunction design of stacked p—n interfaces tuned to different bandwidths has been proposed.[1] Though these *tandem* solar cells display an improved light-harvesting efficiency,[2] they are typically brittle, heavy, and therefore difficult to implement in future flexible electronic devices.

Unlike conventional semiconductor materials, pristine single- and few-layer graphene (FLG) materials have no band gap.[3−6] The gapless energy dispersion allows electron—hole pairs to be generated over a broad light bandwidth from UV to THz.[7] Therefore, the implementation of all-graphene photovoltaics, that is, a device in which both the active area and electrodes are made of graphene materials, could be able to harvest energy over the whole sun light spectrum, while offering unique properties such as ultralight weight (*i.e.*, graphene is just one atom thick), mechanical flexibility, and optical transparency. Therefore, understanding the optoelectronic properties of graphene-based heterostructures is the first step for exploiting the full potential of this carbon material in flexible and transparent photovoltaic devices.

Previous optoelectronic studies on graphene devices have shown that the photothermoelectric effect is at the origin of the measured photovoltage in graphene p—n junctions and in single-bilayer interfaces.[8−10] On the other hand, the photovoltage measured at the graphene—metal interface is due to a built-in electric field near the contact as a result of charge transfer from the metal contact to the graphene.[11−15] These graphene hybrid structures are at the core of a new generation of ultrafast photodetectors with a remarkable high bandwidth (500 GHz), zero source-drain bias (hence zero dark current) operation, and good internal quantum efficiency.[13] However, these devices still employ opaque metallic nanostructures which would introduce significant haze caused by light scattering[16,17] when used in smart windows and mirrors. The leap to all-graphene structures which have a high transparency would enable the development of a new generation of

* Address correspondence to s.russo@exeter.ac.uk.

Received for review February 2, 2013 and accepted April 9, 2013.

Published online April 09, 2013
10.1021/nn4005704

TABLE 1. Summary of the Device Parameters with Number of Layers (N) and Mobility (μ) Expressed in $cm^2 V^{-1} s^{-1}$ Calculated at a Carrier Concentration of 4×10^{12} cm^{-2}

device name	N_{FeCl_3-FLG}	N_{FLG}	μ_{FeCl_3-FLG}	μ_{FLG}
D1	3	3	≈1000	7100

transparent photovoltaic devices which do not suffer from haze.

Here we study the photovoltage generated in novel all-graphene devices based on $FeCl_3$-intercalated few-layer graphene[18] ($FeCl_3$—FLG, dubbed graphexeter) and pristine graphene. The $FeCl_3$ intercalation is known to dope graphene to record high charge carrier densities (up to ≈9×10^{14} cm^{-2}),[18] and it drops the room temperature square resistance of graphene to just a few ohms,[18] making this material the best transparent conductor. At the interface between $FeCl_3$—FLG/graphene, we observe a dominant photovoltage comparable to the signal measured at the graphene/Au interface. We observe a sign reversal of the photovoltage upon sweeping the chemical potential of the pristine FLG through the charge neutrality point, and we show that this is due to the photothermoelectric effect. Our results demonstrate that $FeCl_3$—FLG can replace expensive and opaque metals in photovoltaic architectures, making these structures mechanically flexible and transparent.

The device is fabricated as follows: pristine few-layer graphene is first deposited by mechanical exfoliation onto heavily doped Si/SiO_2 substrate. Raman spectroscopy and optical contrast are used to determine the number of graphene layers as well as their stacking order (see Table 1 and Supporting Information for a summary of the key device parameters). The intercalation with ferric chloride is performed at 360 °C at 2×10^{-4} Torr for 7.5 h following the procedure described by Khrapach *et al.*[18] (also see Methods). During this process, ferric chloride molecules penetrate between the layers of FLG and heavily p-dope it to record high levels of ≈9×10^{14} cm^{-2}. Subsequently, a pristine FLG flake is transferred over the $FeCl_3$—FLG flake following the methods described in refs 19 and 20. Independent multiple electric contacts made by Cr/Au (5 nm/70 nm) to the bottom $FeCl_3$—FLG and top FLG allow the characterization of these novel heterostructures (see Figures 1 and 2a).

Figure 1 shows the schematic of the final device along with the measurement setup. The $FeCl_3$—FLG flake is kept on the ground, while a small dc bias of 0.1 mV is applied to the pristine FLG flake. The graphene photodetector is then illuminated by a 532 nm HeNe laser focused by using a 100× objective to 1.5 μm spot size at a power of 8.2 μW. The beam is chopped at 370 Hz, and the chopper is used as reference to a lock-in amplifier which measures the photovoltage. The heavily doped Si substrate acts as a

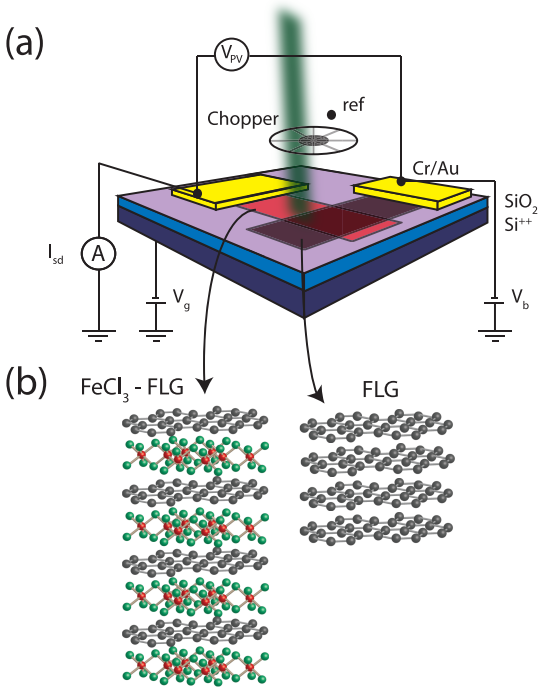

Figure 1. (a) Schematic of the device design and the experimental setup for photovoltage spectroscopy. (b) Crystal structure for fully intercalated $FeCl_3$—FLG and for FLG flakes.

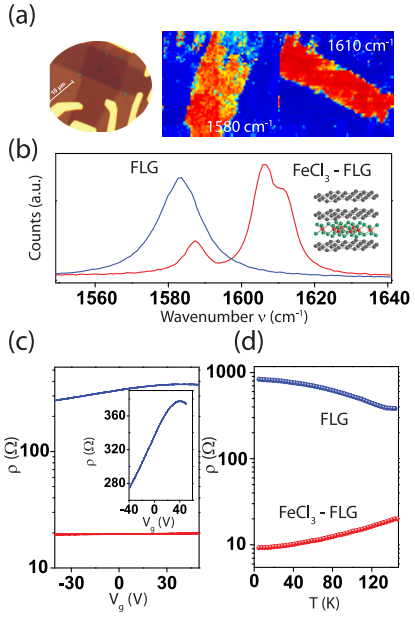

Figure 2. (a) Optical microscope images of a typical device along with the Raman intensity maps for the peaks occurring at 1580 and 1610 cm^{-1} (maximum signal is in red, and zero is in blue in arbitrary units). (b) Plot of the Raman scattering spectrum for the pristine FLG (blue) and the heavily doped $FeCl_3$—FLG (red). The plot in (c) is a graph of resistance *versus* back-gate voltage for $FeCL_3$—FLG (red) and pristine FLG (blue) for device D2 measured at room temperature and zero bias (see Supporting Information). The plot in the inset is a linear scale plot of the resistance *versus* back-gate voltage for the pristine FLG. (d) Temperature dependence of the zero bias resistance for $FeCl_3$ (red) and pristine FLG (blue) at $V_g = 0$ V.

global back-gate which we use to tune the chemical potential of graphene, whereas the resistivity of the $FeCl_3$—FLG flake is unaffected by the typical values of used gate voltage due to the high doping level.[18] The devices are mounted on a scanning stage which allows one to map the photoresponse of these graphene-based heterointerfaces in the x—y directions with a spatial resolution of 1 μm.

RESULTS AND DISCUSSION

To probe the homogeneity of the intercalation, we employ Raman spectroscopy (see Methods). Figure 2a shows a map of the Raman G-band for the non-intercalated and intercalated parts for a typical device. It is apparent that the pristine FLG shows the well-known strong Raman intensity at 1580 cm^{-1} corresponding to the G-band, whereas a strong Raman intensity at 1610 cm^{-1} is present over the whole area of the intercalated FLG, demonstrating the uniformity of the intercalation process. The upshift of the G-band to 1612 and 1625 cm^{-1} has been previously studied and attributed to charge transfer from $FeCl_3$ to graphene.[18,21] More specifically, the shift of the G-band to 1612 cm^{-1} is a signature of a graphene sheet with only one adjacent $FeCl_3$ layer, whereas the shift to 1625 cm^{-1} characterizes a graphene sheet sandwiched between two $FeCl_3$ layers. Figure 2b shows the Raman G-band for the pristine (blue) and intercalated (red) FLG of the device. The pristine FLG is lightly doped as indicated by the Raman G-band appearing at 1583 cm^{-1}.[22,23] On the other hand, the Raman spectrum of the intercalated FLG shows three shifts of the G-band to 1587, 1608, and 1610 cm^{-1}. These observations suggest that the peak at 1610 cm^{-1} originates from two graphene layers sandwiching one layer of $FeCl_3$,[18,21] whereas the other peaks are due to doped pristine graphene layers.[18] Since the intercalated flakes which we chose for these experiments are trilayers, the structure can be understood as a layer of $FeCl_3$ sandwiched between a graphene monolayer and a graphene bilayer, as schematically shown in the inset of Figure 2b.

To further characterize the devices, we study the electrical transport properties of the independently contacted pristine FLG and $FeCl_3$—FLG flakes. Electrical measurements are preformed in constant current using an excitation current of 100 nA in four-terminal configuration to avoid the contact resistance at the interface with metals.[24] A summary of the back-gate and temperature dependence of the resistance of a typical device is presented in Figure 2c,d. The $FeCl_3$—FLG shows no gate control of the resistivity (red curve in Figure 2c), which is typical of heavily doped graphene. On the other hand, the pristine FLG (see blue curve in Figure 2c) exhibits the expected large modulation of resistance as a function of gate voltage and a maximum resistance at $V_g = 40$ V for this specific device. This indicates the presence of residual p-doping probably caused by $FeCl_3$ molecules present on the surface of the underlaying $FeCl_3$—FLG. Consistently, we observe that the $FeCl_3$—FLG has a room temperature resistivity of $\approx$11 Ω which decreases upon lowering the temperature down to 9 Ω at 4.2 K (see Figure 2d). The observed metallic behavior of the resistivity is consistent with the heavy p-doping of the system induced by the intercalation with $FeCl_3$, and it is contrasted by the typical temperature dependence of the pristine FLG, which shows increasing resistivity upon lowering temperature[25] (see Figure 2d).

The optoelectronic properties of these graphene-based hybrid structures are characterized by measuring the photovoltage generated across the pristine FLG/$FeCl_3$—FLG interface while rastering the laser spot over the active device area. Figure 3a shows the photovoltage generated in device D1 as a function of position of the laser beam (see Supporting Information for a similar characterization of another device). It is apparent that there is a strong photovoltage at the Au/FLG (blue) and FLG/$FeCl_3$—FLG (red) interfaces, while the photovoltage at the $FeCl_3$—FLG/Au is nearly 0. To understand the origin of the generated photovoltage, we fixed the position of the laser beam on a specific location of the interfaces, and by changing the back-gate voltage, we modulated the chemical potential from holes to electrons in the pristine FLG. Figure 3b,c shows the gate dependence of the resistance for the different interfaces found in the device as indicated in the graph. In particular, for the pristine flake, the charge neutrality point (CNP) occurs at 20 V and the crossover from hole transport to electron transport can be studied (see Figure 3b,d).

A comparison of the gate dependence (in the range of -50 V $< V_g <$ 70 V) of the photovoltage for all interfaces shows striking differences in the measured signal depending on the interface that is measured (see Figure 3d,e). More specifically, experimentally, we find no detectable photovoltage generated at the Au/$FeCl_3$—FLG (black). This is in contrast to the photovoltage generated at the Au/FLG (blue) and FLG/$FeCl_3$—FLG (red) which is nonzero (up to $\pm$30 mV/W), it is nonmonotonous, it switches sign when the gate voltage drives the Fermi energy accross the charge neutrality point, and it decreases monotonously for very high doping levels. Furthermore, we observe that the photovoltage generated at the Au/FLG is of comparable magnitude to that measured at the FLG/$FeCl_3$—FLG interface but it has opposite sign, that is, negative in the hole side and positive in the electron side. Finally, we note that the photovoltage generated at graphene/$FeCl_3$—FLG is equivalent or larger than what has been previously reported in doubly gated graphene p—n junctions.

The fact that (1) the photovoltage generated at the Au/FLG (blue) and FLG/$FeCl_3$—FLG (red) is nonzero, (2) it is nonmonotonous, (3) it switches sign when the gate voltage drives the Fermi energy across the charge

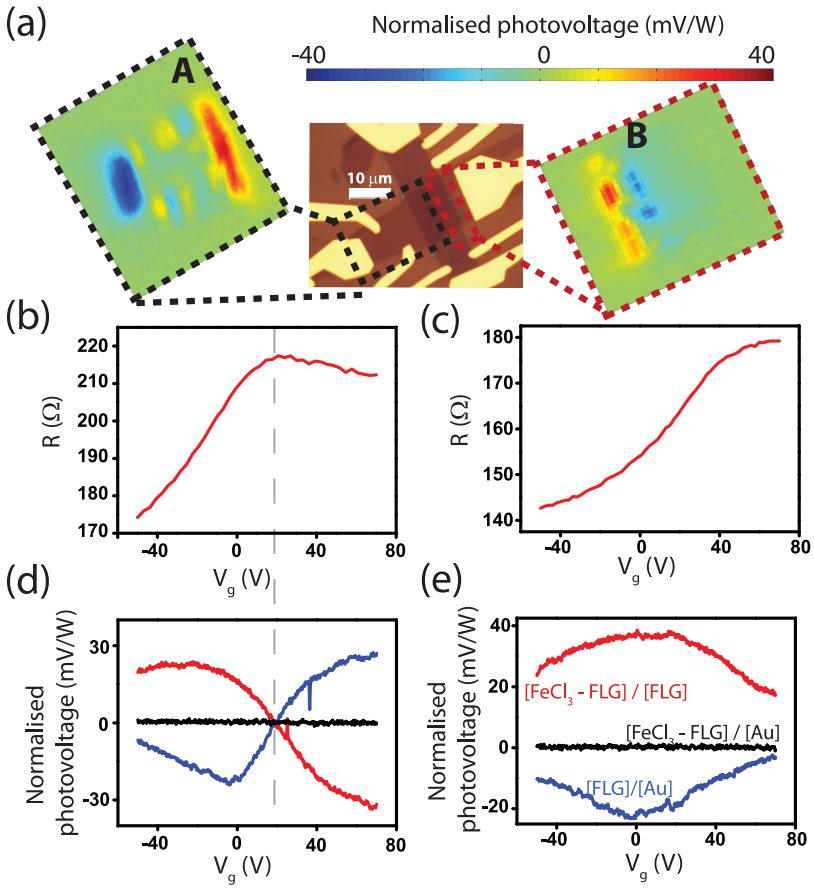

Figure 3. (a) Color-coded photovoltage spectroscopy for the interfaces of the device highlighted in the optical micrograph picture. These measurements are taken for $V_g = 0$ V, 1×10^{-4} V source-drain bias and with a laser power of 8.2 μW. The blue region in the photovoltage maps corresponds to the Au/FLG interface, and the red is the FLG/$FeCl_3$−FLG interface. In these measurements, the Au contact connected to the $FeCl_3$−FLG flake is grounded while the Au contact connected to the FLG is the source. The graphs in (b) and (c) show the gate dependence of the resistance for the interfaces A and B. (d,e) Back-gate dependence of the photovoltage when the laser position is located at the Au/$FeCl_3$−FLG (blue), FLG/$FeCl_3$−FLG (red), and the $FeCl_3$−FLG/Au (black) for the interfaces A and B.

neutrality point, and (4) it decreases monotonously for high doping levels suggests that photothermoelectric effects are at the origin of the observed signal. Similar observations have been previously reported in graphene single-bilayer junctions[8] as well as doubly gated graphene p−n junctions,[9,10] demonstrating the occurrence of photothermoelectric effects later supported by theoretical studies.[26] In the photothermoelectric effect, after the electrons are photoexcited from the valence band to the conduction band, they form a hot Fermion distribution by relaxing back to the Fermi level. When there is a difference in the density of states of the materials forming the photoactive interface, the carriers diffuse from one side to the other of the interface, leading to a photovoltage.[8,9,26,27]

If charge transfer was responsible for the measured photovoltage, the signal should have increased upon increasing the carrier concentrations as the band bending increases.[26,27] This is in contrast with the observed decrease of the photovoltage for high doping of the non-intercalated flake, which is instead expected for photothermoelectric effects. Finally, in our devices, we do not expect the contacts to contribute with significant photovoltaic effects since our interface material is chromium, which is known to induce a very small band bending in graphene.[27−29]

Having established that photothermoelectric effect is at the origin of the observed photovoltage, the measued zero photovoltage at the $FeCl_3$−FLG/Au interface implies that the Seebeck coefficients of $FeCl_3$−FLG are similar to that of Au. This observation, together with the fact that the magnitude of the photovoltage measured at the FLG/Au and FLG/$FeCl_3$−FLG is comparable, demonstrates that $FeCl_3$−FLG is a good replacement for metals or local gates in future graphene photodetectors.

The photovoltage generated by the photothermoelectric effect is $V_{pv} = (S_2 - S1)\Delta T$, where S_i is the Seebeck coefficient of the different materials and ΔT is the temperature difference. The Mott relation gives[30−32]

$$S = -\frac{\pi^2 k_B^2 T}{3e} \frac{1}{G} \frac{dG}{dn} \frac{dn}{dE} \qquad (1)$$

For device D1, the top layer graphene is ABA trilayer graphene (see Supporting Information), and we

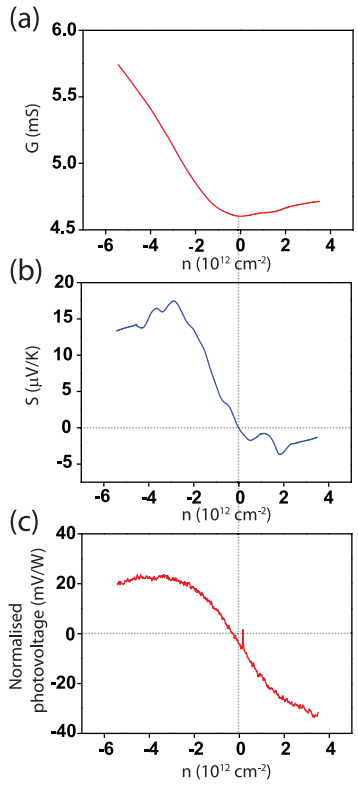

Figure 4. (a) Electrical conductance for the interface A of device D1 (see Figure 3a) as a function of carrier concentration. (b) Graph of the Seebeck coefficient calculated from the data shown in (a) using eq 1. (c) Plot of the photovoltage measured at the FLG/$FeCl_3$−FLG interface.

approximate the $E_f(n)$ dependence to be that of bilayer graphene where[33]

$$E_f = \frac{1}{2}\left((2\hbar v_F)^2\pi n + 2\gamma_1^2 - 2\gamma_1\sqrt{(2\hbar v_F)^2\pi n + \gamma_1^2}\right)^{1/2} \quad (2)$$

Here, γ_1 is the interlayer coupling strength, which we take to be 0.4 eV.[34,35] Figure 4a shows the dependence of the electrical conductance (G) as a function of the charge density (n), where n is extracted from V_g using the plane plate capacitor model. Figure 4b shows the calculated Seebeck coefficient using the measured $G(n)$ and eqs 1 and 2. The measured photovoltage has a similar charge density dependence to the Seebeck coefficient, and both signals cross over from positive to negative at the charge neutrality point (see Figure 4c). This has to be expected when the photothermoelectric effects dominate the measured photovoltage.[8−10] In these devices, only the Seebeck coefficient of the ABA trilayer flake contributes significantly to the photovoltage since the Seebeck coefficient of the $FeCl_3$−FLG is 0 as there is no gate modulation of the resistivity due to the large density of states—that is, $dG/dn \approx 0$ for our available gate voltage range. Furthermore, Figure 4b,c shows that the Seebeck coefficient and the measured photovoltage are not exactly proportional. This discrepancy can be attributed to the local differences in the magnitude of the Seebeck coefficient induced by inhomogeneous doping of the ABA trilayer graphene flake since the photovoltage is a probe of the local density of states.[8]

CONCLUSIONS

In summary, we show that the $FeCl_3$−FLG can be used as a replacement for metal contacts in graphene photodetectors. The high degree of doping in $FeCl_3$−FLG makes the resistivity of this material insensitive to a global gate voltage acting on the pristine graphene; therefore, $FeCl_3$−FLG is an ideal conductive interconnect material. Our experiments demonstrate that $FeCl_3$−FLG can replace metals in a new generation of all-graphene-based photodetectors. In particular, we demonstrate a maximum photovoltage of ≈0.1 V/W at the FLG/$FeCl_3$−FLG interface. We attribute the measured photovoltage to the photothermoelectric effect with a maximum Seebeck coefficient of 20 μV/K for ABA trilayer graphene.

METHODS

Intercalation with $FeCl_3$. The intercalation process with $FeCl_3$ is performed by placing both the anhydrous $FeCl_3$ powder and the substrates with pristine few-layer graphene in vacuum (∼10−4 mbar) and at 310 and 350 °C for 7.5 h. A heating rate of 10 °C/min is used during the warming and cooling of the two zones.

Raman Spectroscopy. Raman spectra are collected in ambient air and at room temperature with a Renishaw spectrometer. An excitation laser with a wavelength of 532 nm, focused to a spot size of 1.5 μm diameter and a ∼100× objective lens, is used. To avoid sample damage or laser-induced heating, the incident power is kept at 5 mW.

Conflict of Interest: The authors declare no competing financial interest.

Acknowledgment. S.R. and M.F.C. acknowledge financial support from EPSRC (Grant Nos. EP/G036101/1 and EP/J000396/1).

Supporting Information Available: Addional experimental details, figures, and tables. This material is available free of charge *via* the Internet at http://pubs.acs.org.

REFERENCES AND NOTES

1. Kim, J. Y.; Lee, K.; Coates, N. E.; Moses, D.; Nguyen, T.-Q.; Dante, M.; Heeger, A. J. Efficient Tandem Polymer Solar Cells Fabricated by All-Solution Processing. *Science* **2007**, *317*, 222–225.
2. Tanabe, K. Review of Ultrahigh Efficiency III−V Semiconductor Compound Solar Cells: Multijunction Tandem, Lower Dimensional, Photonic Up/Down Conversion and Plasmonic Nanometallic Structures. *Energies* **2009**, *2*, 504–530.
3. Geim, A. K.; Novoselov, K. S. The Rise of Graphene. *Nat. Mater.* **2007**, *6*, 183–191.
4. Craciun, M. F.; Russo, S.; Yamamoto, M.; Tarucha, S. Tuneable Electronic Properties in Graphene. *Nano Today* **2011**, *6*, 42–60.

5. Novoselov, K. S.; Geim, A. K.; Morozov, S. V.; Jiang, D.; Katsnelson, M. I.; Grigorieva, I. V.; Dubonos, S. V.; Firsov, A. A. Two-Dimensional Gas of Massless Dirac Fermions in Graphene. *Nature* **2005**, *438*, 197–200.
6. Khodkov, T.; Withers, F.; Hudson, D. C.; Craciun, M. F.; Russo, S. Electrical Transport in Suspended and Double Gated Trilayer Graphene. *Appl. Phys. Lett.* **2012**, *100*, 013114.
7. Dawlaty, J. M.; Shivaraman, S.; George, P.; Cahndrashekhar, M.; Rana, F.; Spencer, M. G.; Veksler, D.; Chen, Y. Measurement of the Optical Absorption Spectra of Epitaxial Graphene from Terahertz to Visible. *Appl. Phys. Lett.* **2008**, *93*, 131905.
8. Xu, X.; Gabor, N. M.; Alden, J. S.; van der Zande, A. M.; McEuen, P. L. Photo-Thermoelectric Effect at a Graphene Interface Junction. *Nano Lett.* **2010**, *10*, 562–566.
9. Lemme, M. C.; Koppens, F. H. L.; Falk, A. L.; Rudner, M. S.; Park, H.; Levitov, L. S.; Marcus, C. M. Gate-Activated Photoresponse in a Graphene p−n Junction. *Nano Lett.* **2011**, *11*, 4134–4137.
10. Gabor, N. M.; Song, J. C. W.; Ma, Q.; Nair, N. L.; Taychatanapat, T.; Watanabe, K.; Taniguchi, T.; Levitov, L. S.; Jarillo-Herrero, P. Hot Carrier-Assisted Intrinsic Photoresponse in Graphene. *Science* **2011**, *334*, 648–652.
11. Surajit, G.; Biddut, K. S.; Anindarupa, C.; Lei, Z.; Saiful, I. K. Position Dependent Photodetector from Large Area Reduced Graphene Oxide Thin Films. *Appl. Phys. Lett.* **2010**, *96*, 163109.
12. Park, J.; Ahn, Y. H.; Ruiz-Vargas, C. Imaging of Photocurrent Generation and Collection in Single-Layer Graphene. *Nano Lett.* **2009**, *9*, 1742–1746.
13. Xia, F.; Mueller, T.; Lin, Y.; Valdes-Garcia, A.; Avouris, P. Ultrafast Graphene Photodetector. *Nat. Nanotechnol.* **2009**, *4*, 839–843.
14. Mueller, T.; Xia, F.; Avouris, P. Graphene Photodetectors for High-Speed Optical Communications. *Nat. Photonics* **2010**, *4*, 297–301.
15. Nazin, G.; Zhang, Y.; Zhang, L.; Sutter, E.; Sutter, P. Visualization of Charge Transport through Landau Levels in Graphene. *Nat. Phys.* **2010**, *6*, 870–874.
16. De, S.; Boland, C. S.; King, P. J.; Sorel, S.; Lotya, M.; Patel, U.; Xiao, Z. L.; Coleman, J. N. Transparent Conducting Films from $NbSe_3$ Nanowires. *Nanotechnology* **2011**, *22*, 285202.
17. Hecht, D. S.; Hu, L.; Irvin, G. Emerging Transparent Electrodes Based on Thin Films of Carbon Nanotubes, Graphene, and Metallic Nanostructures. *Adv. Mater.* **2011**, *23*, 1482–1513.
18. Khrapach, I.; Withers, F.; Bointon, T. H.; Polyushkin, D. K.; Barnes, W. L.; Russo, S.; Craciun, M. F. Novel Highly Conductive and Transparent Graphene-Based Conductors. *Adv. Mater.* **2012**, *24*, 2844–2849.
19. Dean, C. R.; Young, A. F.; Meric, I.; Lee, C.; Wang, L.; Sorgenfrei, S.; Watanabe, K.; Taniguchi, T.; Kim, P.; Shepard, K. L.; *et al.* Boron Nitride Substrates for High-Quality Graphene Electronics. *Nat. Nanotechnol.* **2010**, *5*, 722–726.
20. Britnell, L.; Gorbachev, R. V.; Jalil, R.; Belle, B. D.; Schedin, F.; Mishchenko, A.; Georgiou, T.; Katsnelson, M. I.; Eaves, L.; Morozov, S. V.; *et al.* Field-Effect Tunneling Transistor Based on Vertical Graphene Heterostructures. *Science* **2012**, *335*, 947–950.
21. Zhao, W.; Tan, P. H.; Liu, J.; Ferrari, A. C. Intercalation of Few-Layer Graphite Flakes with $FeCl_3$: Raman Determination of Fermi Level, Layer by Layer Decoupling, and Stability. *J. Am. Chem. Soc.* **2011**, *133*, 5941–5946.
22. Ferrari, A. C.; Meyer, J. C.; Scardaci, V.; Casiraghi, C.; Lazzeri, M.; Mauri, F.; Piscanec, S.; Jiang, D.; Novoselov, K. S.; Roth, S.; *et al.* Raman Spectrum of Graphene and Graphene Layers. *Phys. Rev. Lett.* **2006**, *97*, 187401.
23. Malard, L. M.; Pimenta, M. A.; Dresselhaus, G.; Dresselhaus, M. S. Raman Spectroscopy in Graphene. *Phys. Rep.* **2009**, *473*, 51–87.
24. Russo, S.; Craciun, M. F.; Yamamoto, M.; Morpurgo, A. F.; Tarucha, S. Contact Resistance in Graphene-Based Device. *Physica E* **2010**, *42*, 677–679.
25. Zhu, W.; Perebeinos, V.; Freitag, M.; Avouris, P. Carrier Scattering, Mobilities, and Electrostatic Potential in Monolayer, Bilayer, and Trilayer Graphene. *Phys. Rev. B* **2009**, *80*, 235402.
26. Song, J. C. W.; Rudner, M. S.; Marcus, C. M.; Levitov, L. S. Hot Carrier Transport and Photocurrent Response in Graphene. *Nano Lett.* **2011**, *11*, 4688–4692.
27. Xia, F.; Mueller, T.; Golizadeh-Mojarad, R.; Freitag, M.; Lin, Y.; Tsang, J.; Perebeinos, V.; Avouris, P. Photocurrent Imaging and Efficient Photon Detection in a Graphene Transistor. *Nano Lett.* **2009**, *9*, 1039–1044.
28. Pinto, H.; Jones, R.; Goss, J. P.; Briddon, P. R. Unexpected Change in the Electronic Properties of the Au−Graphene Interface Caused by Toluene. *Phys. Rev. B* **2010**, *82*, 125407.
29. Giovannetti, G.; Khomyakov, P. A.; Brocks, G.; Karpan, V. M.; van den Brink, J.; Kelly, P. J. Doping Graphene with Metal Contacts. *Phys. Rev. Lett.* **2008**, *101*, 026803.
30. Cutler, M.; Mott, N. F. Observation of Anderson Localization in an Electron Gas. *Phys. Rev.* **1969**, *181*, 1336–1340.
31. Wei, P.; Bao, W.; Pu, Y.; Lau, C. N.; Shi, J. Anomalous Thermoelectric Transport of Dirac Particles in Graphene. *Phys. Rev. Lett.* **2009**, *102*, 166808.
32. Zuev, Y. M.; Chang, W.; Kim, P. Thermoelectric and Magnetothermoelectric Transport Measurements of Graphene. *Phys. Rev. Lett.* **2009**, *102*, 096807.
33. Castro Neto, A. H.; Guinea, F.; Peres, N. M. R.; Novoselov, K. S.; Geim, A. K. The Electronic Properties of Graphene. *Rev. Mod. Phys.* **2009**, *81*, 109–162.
34. Nilsson, J.; Neto, A. H. C.; Guinea, F.; Peres, N. M. R. Electronic Properties of Graphene Multilayers. *Phys. Rev. Lett.* **2006**, *97*, 266801.
35. McCann, E.; Abergel, D. S. L.; Falko, V. I. Electrons in Bilayer Graphene. *Solid State Commun.* **2007**, *143*, 110–115.